Deep subwavelength flow-resonant modes in a waveguide-coupled plasmonic nanocavity

Ji-Song Pae, Song-Jin Im ⬤,* Kil-Song Song, Chol-Song Ri, Kum-Song Ho, and Yong-Ha Han

Department of Physics, Kim Il Sung University, Taesong District, 02-381-4410 Pyongyang, Democratic People's Republic of Korea

The waveguide-coupled plasmonic nanocavity is known to be a deep subwavelength platform that combines on-chip compatibility with a strong light-matter interaction at the resonance of local field enhancement; however, the resonant local field enhancement provides no magneto-optical activity. We conceptually investigate the deep subwavelength flow-resonant modes of the waveguide-coupled plasmonic nanocavity at which the local field enhancement deviates from the strongest and, instead, the power flow reaches its maximum. These flow-resonant modes exhibit resonant enhancements of magneto-optical activity and the inverse Faraday effect. Frequency-selective enhancement of light-magnetization interaction at the flow-resonant modes allows us to propose multichannel all-optical writing and reading of magnetic bits in nanophotonic integrated circuits. Our findings would open the way towards on-chip deep subwavelength magneto-optical devices and opto-magnetic recording with a great potential for high-speed on-chip memory.

Magnetoplasmonic nanostructures with combined plasmonic and magnetic properties is appealing for enhancing interaction between light and magnetization in nanosystems. Research on this fast emerging topic has resulted in a considerable number of experimental and theoretical papers (for reviews, see Ref. [1]). Many of their configurations require the free-space coupling scheme and thus are relatively bulky and not compatible with on-chip integration. Recently, magneto-optical disk resonators coupled to plasmonic waveguides [2,3] were proposed to enhance light-magnetization interactions in a compact configuration. However, this approach is based on a traveling mode and thus it has a multiwavelength scale. Integrating a plasmonic waveguide [4] and a deep subwavelength nanocavity [5–7] is a well-known approach for fully integrated nanophotonic devices compatible with on-chip integration. In spite of intensive work [8–13] to enhance and manipulate light-matter interactions at the nanometer scale based on the conception of plasmonic nanocavity-waveguide coupling, to our knowledge, so far, no work has been presented to propose deep subwavelength magneto-optical (MO) devices based on this conception.

The development of the next-generation magnetic memory devices will be driven by the demand for ultrafast and high-density recording. All-optical magnetic recording has become a topic of strong scientific interest at the crossroads of photonics and magnetism because of its potential impact for magnetic memory devices with unprecedented speed [14]. The request to increase the recording density and decrease the lowest requested pulse energy motivated studies for nanoscale-confined all-optical magnetization switching assisted by plasmonic nanostructures [15–18]. Recently, we

reported that all-optical magnetization switching due to the inverse Faraday effect (IFE) is achievable with surface plasmon polaritons propagating along plasmonic waveguides without the need of free-space coupling of circularly polarized light [19,20].

The conventional resonant mode of plasmonic nanocavity with the strong local field enhancement does not exhibit MO activity, which is why the conception of the plasmonic nanocavity-waveguide coupling has never been proposed for deep subwavelength MO devices. In this paper we conceptually investigate the flow-resonant modes of the waveguide-coupled plasmonic nanocavity. The flow-resonant modes are distinguished from the conventional resonant mode at which the coupled energy and the field enhancement reach their maxima. At the flow-resonant modes, the field enhancement deviates from the strongest and, instead, the power flow inside the cavity reaches its maxima. We note that the flow-resonant modes are inherent in a single cavity coupled to a waveguide and they are distinguished from the well-studied resonance-splitting phenomena [21] in multicavities. These flow-resonant modes are suitable for frequency-selective enhanced interaction between light and magnetization, which exhibit resonant enhancements of MO activity and as its counterpart, the IFE. Multichannel all-optical magnetic recording with nanometer resolution is proposed based on multicavity simultaneous excitation of the flow-resonant modes in a magnetoplasmonic nanocavity array with one multicolor pulse which allows us to much increase the writing and reading speeds many times by better utilizing excessive optical bandwidth, as is similarly done in wavelength division multiplexing (WDM) optical communications.

The geometry of a plasmonic rectangular nanocavity side-coupled to metal-insulator-metal (MIM) waveguide is shown in Fig. 1(a). The standing-wave mode resonance exhibits the strongest field enhancement in the plasmonic nanocavity [the
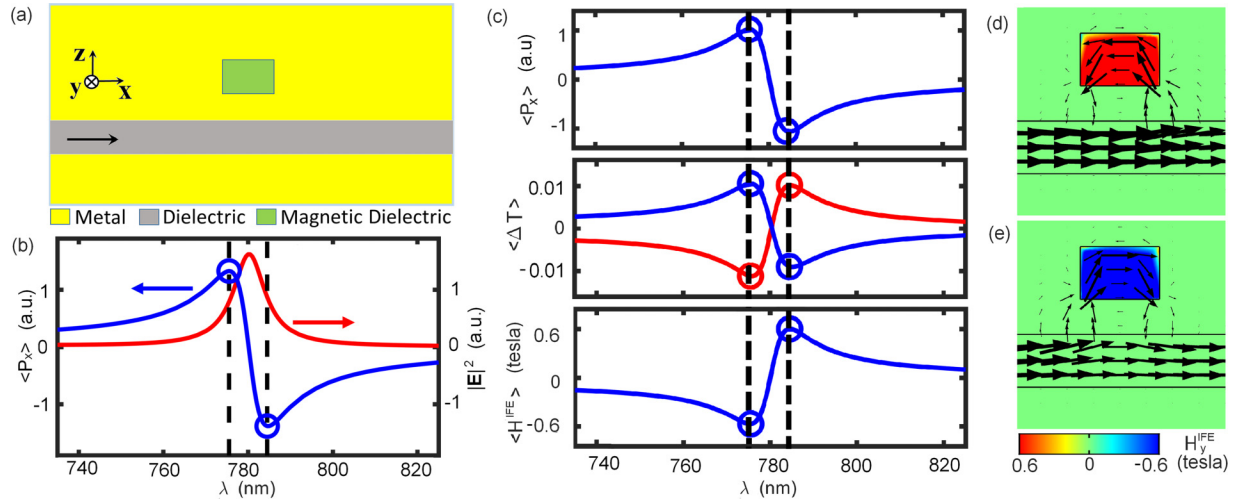
*sj.im@ryongnamsan.edu.kp

FIG. 1. Resonances of power flow in a plasmonic nanocavity. (a) The geometry of a plasmonic nanocavity side-coupled to a metal-insulator-metal (MIM) waveguide. The plasmonic nanocavity is filled with a MO material. (b) Spectral dependence of the average power flow $\langle P_x \rangle$ along the direction of x-axis (blue curve) and the average electric field intensity $\langle |\vec{E}|^2 \rangle$ (red curve) over the plasmonic nanocavity. Circles mark the double flow-resonant peaks. (c) Spectral dependence of the average power flow $\langle P_x \rangle$ along the direction of the x axis, the transmission shift ΔT through the MIM waveguide by an external magnetic field along the direction of the y axis which manifests the MO activity of the plasmonic nanocavity and the average effective magnetic field $\langle H_y^{\text{IFE}} \rangle$ by the inverse Faraday effect (IFE). The brackets $\langle \cdot \rangle$ denote the average value over the plasmonic nanocavity [the green part of panel (a)]. (d), (e) Near-field distributions of the IFE-induced magnetic field $\langle H_y^{\text{IFE}} \rangle$ (colors) and the power flow $\vec{P}$ (black arrows) at the double flow-resonant frequencies in the plasmonic nanocavity. The arrow size is proportional to the magnitude of the power flow and the arrow direction is along the direction of the power flow. The power flow is calculated by $\vec{P} = \frac{1}{2}\text{Re}(\vec{E}^* \times \vec{H})$. In our calculation example we assumed a thickness of 30 nm of the waveguide, a height of 30 nm, and a length of 45 nm of the rectangular nanocavity and a distance of 20 nm between the waveguide and the nanocavity. Also, we assumed the permittivity of air ($\varepsilon_{\text{air}} = 1$) as the permittivity of the dielectric, the experimental data of the permittivity of silver [22] as the permittivity of the metal and the experimental data of the permittivity and the MO susceptibility of Bi-substituted iron garnet (BIG) [23] as those of the magnetic dielectric ($\varepsilon_r = 8$, $\alpha = 5.5 \times 10^{-7}$ m/A). For the second panel of (c) we assumed the gyration $g = 0.06$ (the red curve) and $g = -0.06$ (the blue curve) [24] in the presence of an external magnetic field along the direction of the y axis and its opposite direction, respectively. For the numerical calculations of the IFE we assumed the incident mode power through the MIM waveguide to be 10 W/μm.

red curve of Fig. 1(b)], which has been widely used for enhancing light-matter interactions at the nanometer scale; however, it exhibits the zero value of the average power flow $\langle P_x \rangle$ along the direction of x axis over the plasmonic nanocavity [the blue curve of Fig. 1(b)]. The power flow is calculated by $\vec{P} = \frac{1}{2}\text{Re}(\vec{E}^* \times \vec{H})$, which is known as the Poynting vector. The averaged power flow $\langle P_x \rangle$ over the plasmonic nanocavity has double resonant peaks in the vicinity of the standing-wave mode resonance, although the average field intensity $\langle |\vec{E}^2| \rangle$ deviates from the strongest. Here, a power flow is introduced only to the left terminal of the waveguide. The feeding condition of the waveguide is asymmetric, thus a power flows through the waveguide. However, at the resonance, the power flow through the cavity is exactly zero because, at the resonance, the standing-wave mode is constructed in the cavity. We note that the well-known single peak in transmission spectrum which is explained by using the temporal coupled-mode theory (see Supplemental Material [25] and Ref. [26]) corresponds to the peak in the field intensity curve [the red curve of Fig. 1(b)]. The resonant wavelength can be manipulated by changing the cavity sizes: the cavity length and width (see Supplemental Material [25]). Its dependance on the cavity sizes is explained by the standing-wave mode resonance condition in the MIM nanocavity [27]. The bandwidth of the resonance can be controlled by adjusting the distance between the plasmonic waveguide and cavity

(see Supplemental Material [25]). This is attributed to the escape rate γ_e significantly changing by adjusting the distance between the plasmonic waveguide and cavity [28]. The larger distance supports the narrower bandwidth; however, it suffers from the smaller power flow. In contrast, the smaller distance suffers from the larger bandwidth which can induce detrimental interactions with other cavity modes. Thus, we assumed a moderate distance of 20 nm for cavity-selective coupling with a multicavity array.

The second panel of Fig. 1(c) shows the transmission shift $\Delta T = T - T_0$ through the MIM waveguide by an external magnetic field along the direction of the y axis, where T and T_0 are the transmission in the presence of the external magnetic field and the one in the absence of the external magnetic field, respectively. Under the presence of the external magnetic field, the permittivity tensor of magnetic dielectric filling the nanocavity is expressed as

$$\hat{\varepsilon} = \begin{pmatrix} \varepsilon_r & 0 & -ig \\ 0 & \varepsilon_r & 0 \\ ig & 0 & \varepsilon_r \end{pmatrix}. \tag{1}$$

Here, the gyration $g = \alpha M$ is proportional to the magnetization M, where α is the MO susceptibility. While at the resonance with the strongest field enhancement the transmission shift ΔT becomes zero, at the two resonances of power flow

the transmission shift ΔT reaches its positive and negative peaks, respectively. The transmission shift ΔT manifesting the MO activity and measurable in the far field is sign-changed by magnetic-field reversal, which is promising for all-optical reading of a magnetic bit at the nanometer scale. For the numerical calculations we assumed the gyrations $g = 0.06$ (the red curve) and $g = -0.06$ (the blue curve) for the cases of the external magnetic fields along the direction of the y axis and along its opposite direction, respectively. Next we consider the IFE, which is the counterpart of the MO effect. The rotating electric-field vector of a transverse magnetic (TM) plasmonic mode can act as an effective magnetic field along the transverse y direction due to the IFE, which is expressed as follows [29,30]:

$$H_y^{\mathrm{IFE}} = -i\varepsilon_0 \alpha (E_x^* E_z - E_x E_z^*). \tag{2}$$

As shown in the third panel of Fig. 1(c) the average IFE-induced magnetic field $\langle H_y^{\mathrm{IFE}} \rangle$ over the nanocavity has resonant peaks at two wavelengths which coincide with the double flow-resonant wavelengths. The IFE-induced magnetic field is switchable in sign by changing the frequency from one to another of the two resonance frequencies. These facts show that the double flow-resonant modes are suitable for enhancing the interaction between light and magnetization at the nanometer scale. Here, we note that the sign reversal of power flow is not a result of magnetization. It is a result of waveguide-cavity coupling without magnetization; however, it is very promising for enhancing the MO effect and as its counterpart, the IFE.

Now we consider a plasmonic nanocavity array side-coupled to the MIM waveguide. The geometry is shown in the first panel of Fig. 2(a). Here the resonant wavelengths of the nanocavities can be manipulated by the cavity sizes. In our calculation example the cavity lengths have been appropriately manipulated to provide standing-wave resonances of 780, 840, and 900 nm, respectively. In the first panel of Fig. 2(b) the MO activity of the plasmonic nanocavity array is manifested by the transmission shift ΔT through the MIM waveguide by an external magnetic field. The transmission shift ΔT reaches the extrema with both positive and negative signs at the wavelengths of λ_n^0 and λ_n^1 ($n = 1$, 2, and 3), respectively. Here λ_n^0 and λ_n^1 are the double flow-resonant wavelengths of the nth cavity, respectively. It is predicted that multicavity magnetization states can be read simultaneously by measuring channel transmissions $\Delta T(\lambda_n^0)$ or $\Delta T(\lambda_n^1)$ of a multicolor pulse. In the second panel of Fig. 2(b) the IFE-induced magnetic field in the nth cavity has resonant peaks at two wavelengths which coincide with the double flow-resonant wavelengths of the nth cavity, respectively. The IFE-induced magnetic field is switchable in sign by changing the frequency from one to another of the double flow-resonant frequencies.

Figure 3 shows distributions of the effective magnetic field induced by the IFE in the nanocavity array. The magnetic bits (p_1, p_2, p_3) manifested by the magnetic states of the nanocavities can be written with an incident multicolor pulse of the wavelengths $(\lambda_1^{p_1}, \lambda_2^{p_2}, \lambda_3^{p_3})$. Here, p_n is 0 or 1, which is a magnetic bit in the nth cavity. Multicavity simultaneous excitation of flow-resonant modes in m cavities with a multicolor pulse of wavelengths of $(\lambda_1^{p_1}, \lambda_2^{p_2}, \ldots, \lambda_m^{p_m})$ enables
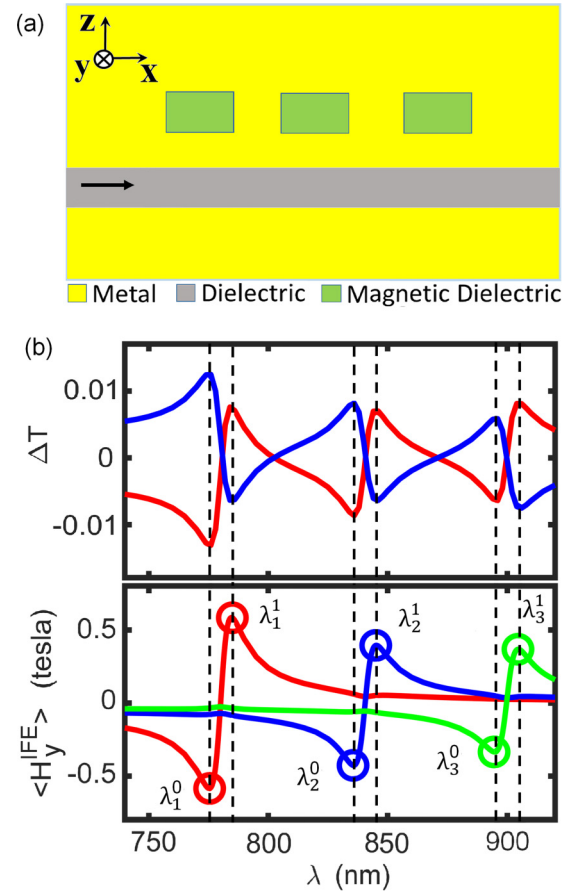

FIG. 2. Power-flow resonances in a plasmonic nanocavity array. (a) The geometry of a plasmonic nanocavity array side-coupled to a MIM waveguide. The plasmonic nanocavities are filled with a MO material. First panel of (b) shows the spectral dependence of the transmission shift ΔT through the MIM waveguide by an external magnetic field along the direction of the y axis which manifests the MO activity of the nanocavity. Second panel of (b) shows the average effective magnetic fields $\langle H_y^{\mathrm{IFE}} \rangle$ by the IFE over the first (red curve), the second (blue curve), and the third (green curve) nanocavities. λ_n^0 and λ_n^1 are flow-resonant wavelengths of the nth cavity. Lengths of 45.1, 52.5, and 59.8 nm of the nanocavities have been assumed to provide standing-wave resonances of 780, 840, and 900 nm, respectively. A distance of 80 nm between the nanocavities has been assumed. Other parameters are the same as in Fig. 1.

multichannel writing of magnetic bits of $(p_1, p_2, \ldots, p_m)$ with increasing speed by m times.

Table I shows transmissions through the waveguide side-coupled to the nanocavity array with the magnetizations (M_1, M_2, M_3) corresponding to the magnetic bits (p_1, p_2, p_3). p_1 is read as 0 for $T_1 \leqslant 0.73$ and as 1 for $T_1 > 0.73$. p_2 is read as 0 for $T_2 \leqslant 0.75$ and as 1 for $T_2 > 0.75$. p_3 is read as 0 for $T_3 \leqslant 0.74$ and as 1 for $T_3 > 0.74$. The blue and red font colors represent the reading results 0 and 1, respectively. The reading results $[T_1]$, $[T_2]$, and $[T_3]$ coincide with the magnetic bits $p_1 = [M_1]$, $p_2 = [M_2]$, and $p_3 = [M_3]$, respectively.

Finally we would like to discuss that the conceptual suggestion based on the flow-resonant modes is very promising for high-speed on-chip memory. The problem of very fast switching the magnetization emerged recently as one of the
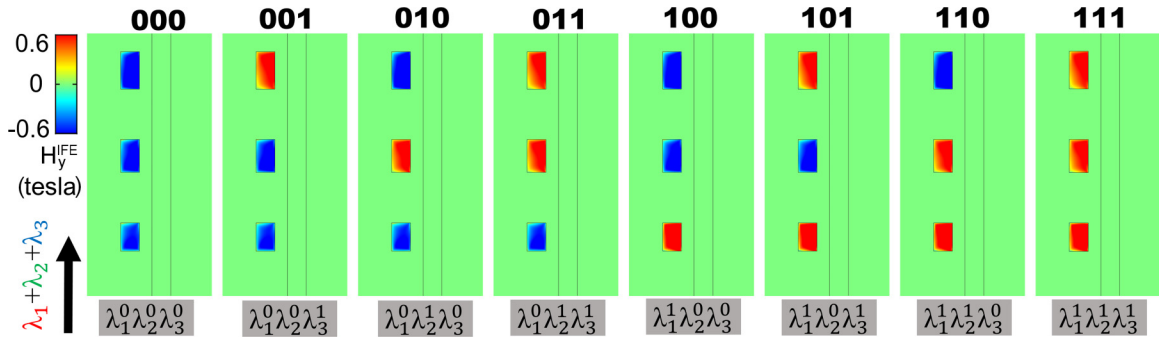
FIG. 3. Writing of multichannel all-optical magnetic recording. Distributions of the effective magnetic field induced by the IFE in the nanocavity array. The magnetic bits (p_1, p_2, p_3) manifested by the magnetic states of the nanocavities have been written with an incident multicolor pulse of the wavelengths $(\lambda_1^{p_1}, \lambda_2^{p_2}, \lambda_3^{p_3})$. Here, p_n is 0 or 1, which is a magnetic bit in the nth cavity. Other parameters are the same as in Fig. 1.

most exciting topics. Usually it takes longer than picoseconds to switch magnetization. In spite of recent studies demonstrating magnetization switching with a subpicosecond laser pulse, optical bandwidth is still excessive [14]. In Fig. 3, a three-wavelength pulse at once interacts with the three cavities. Each one of the three cavities interacts with one wavelength component of the multicolor pulse, respectively. Because a one-wavelength pulse can achieve one-bit recording, a three-wavelength pulse can achieve three-bit recording. For example, we can achieve a writing speed of 1 ps with a three-channel (three-wavelength) 3-ps-duration pulse. On the other hand, most of the already-proposed configurations for all-optical writing and reading of magnetic bits require the free-space coupling scheme and thus are bulky and not compatible with on-chip integration. The waveguide-coupled plasmonic structures are promising for on-chip integration with conventional dielectric waveguides, a feature necessary for future photonic nanocircuits. In particular, the MIM structures that allow for deep subwavelength optical modes have a great potential for on-chip integration with a silicon waveguide, resulting in compact devices suitable for dense integration (a detail discussion can be seen in Ref. [31]). The efficient coupling between a MIM waveguide and a standard silicon waveguide has also been experimentally confirmed [32]. However, the conception of the plasmonic nanocavity-waveguide coupling has never been proposed for resonant enhancements of MO activity and as its counterpart, the IFE, because the conventional resonant mode of plasmonic

nanocavity with the strong local field enhancement does not exhibit MO activity and does not induce the IFE. The conception of the flow-resonant modes of the waveguide-coupled plasmonic nanocavity are suitable for on-chip MO devices and all-optical magnetization switching.

In conclusion, we conceptually investigated the double flow-resonant modes in the waveguide-coupled plasmonic nanocavity at which the power flow in the nanocavity reaches its maxima. While at the resonance of local field enhancement which has been widely used to enhance light-matter interactions at the nanometer scale no power flow and no MO activity are observed, at the two resonances of power flow the strongest enhancements of MO activity and the IFE are observed. The resonant MO activity of the nanocavity is manifested by a transmission shift through the waveguide coupled to the nanocavity under the presence of external magnetic field. The transmission shift is measurable in the far field and is sign-changed by magnetic-field reversal. Reversal of the IFE-induced magnetic field is provided by changing the frequency from one to another of the double flow-resonant frequencies. We also proposed on-chip multichannel all-optical magnetic recording by multicavity simultaneous excitation of the flow-resonant modes in a nanocavity array with one multicolor pulse, which allows us to significantly increase the writing and reading speeds by better utilizing the excessive optical bandwidth. Our findings open the way toward on-chip integration of deep subwavelength MO devices and optomagnetic recording.

TABLE I. Reading of multichannel all-optical magnetic recording. Transmissions through the waveguide side-coupled to the nanocavity array with the magnetizations (M_1, M_2, M_3) corresponding to the magnetic bits (p_1, p_2, p_3). We assumed the gyrations $g = -0.06$ and $g = 0.06$ for the magnetic bits 0 and 1 in the nanocavities, respectively. The magnetic bit p_n in the nth cavity can be read by measuring the transmission $T_n = T(\lambda_n^0)$ at the wavelength λ_n^0 which is the shorter wavelength among the double flow-resonant wavelengths of the nth cavity. p_1 is read as 0 for $T_1 \leqslant 0.73$ and as 1 for $T_1 > 0.73$. p_2 is read as 0 for $T_2 \leqslant 0.75$ and as 1 for $T_2 > 0.75$. p_3 is read as 0 for $T_3 \leqslant 0.74$ and as 1 for $T_3 > 0.74$. The bold and regular fonts represent the reading results 0 and 1, respectively.

$p_1\ p_2\ p_3$	000	001	010	011	100	101	110	111
T_1	**0.719**	**0.720**	**0.722**	**0.723**	0.740	0.742	0.743	0.745
T_2	**0.745**	**0.748**	0.762	0.764	**0.743**	**0.746**	0.760	0.762
T_3	**0.738**	0.753	**0.736**	0.751	**0.737**	0.752	**0.736**	0.750
$[T_1][T_2][T_3]$	000	001	010	011	100	101	110	111

[1] G. Armelles, A. Cebollada, A. García-Martín, and M. U. González, Adv. Opt. Mater. **1**, 10 (2013).

[2] J.-S. Pae, S.-J. Im, K.-S. Ho, C.-S. Ri, S.-B. Ro, and J. Herrmann, Phys. Rev. B **98**, 041406(R) (2018).

[3] J.-S. Pae, S.-J. Im, C.-S. Ri, K.-S. Ho, G.-S. Song, Y.-H. Han, and J. Herrmann, Phys. Rev. B **100**, 041405(R) (2019).

[4] S. I. Bozhevolnyi, V. S. Volkov, E. Devaux, J. Y. Laluet, and T. W. Ebbesen, Nature (London) **440**, 508 (2006).

[5] M. Kuttge, F. J. G. de Abajo, and A. Polman, Nano Lett. **10**, 1537 (2010).

[6] X. L. Zhu, Y. Ma, J. S. Zhang, J. Xu, X. F. Wu, Y. Zhang, X. B. Han, Q. Fu, Z. M. Liao, L. Chen, and D. P. Yu, Phys. Rev. Lett. **105**, 127402 (2010).

[7] X. L. Zhu, J. S. Zhang, J. Xu, and D. P. Yu, Nano Lett. **11**, 1117 (2011).

[8] Z. F. Yu, G. Veronis, S. H. Fan, and M. L. Brongersma, Appl. Phys. Lett. **92**, 041117 (2008).

[9] C. J. Min and G. Veronis, Opt. Express **17**, 10757 (2009).

[10] H. Lu, X. M. Liu, L. R. Wang, Y. K. Gong, and D. Mao, Opt. Express **19**, 2910 (2011).

[11] G. X. Wang, H. Lu, X. M. Liu, and Y. K. Gong, Nanotechnol. **23**, 444009 (2012).

[12] S.-J. Im and G.-S. Ho, Laser Phys. Lett. **12**, 045902 (2015).

[13] C. Lin and A. S. Helmy, Sci. Rep. **5**, 12313 (2015).

[14] A. Kirilyuk, A. V. Kimel, and T. Rasing, Rev. Mod. Phys. **82**, 2731 (2010).

[15] B. C. Stipe, T. C. Strand, C. C. Poon, H. Balamane, T. D. Boone, J. A. Katine, J. L. Li, V. Rawat, H. Nemoto, A. Hirotsune, O. Hellwig, R. Ruiz, E. Dobisz, D. S. Kercher, N. Robertson, T. R. Albrecht, and B. D. Terris, Nat. Photonics **4**, 484 (2010).

[16] T. Liu, T. Wang, A. H. Reid, M. Savoini, X. Wu, B. Koene, P. Granitzka, C. E. Graves, D. J. Higley, Z. Chen, G. Razinskas, M. Hantschmann, A. Scherz, J. Stohr, A.Tsukamoto, B. Hecht, A. V. Kimel, A. Kirilyuk, T. Rasing, and H. A. Durr, Nano Lett. **15**, 6862 (2015).

[17] A. L. Chekhov, A. I. Stognij, T. Satoh, T. V. Murzina, I. Razdolski, and A. Stupakiewicz, Nano Lett. **18**, 2970 (2018).

[18] D. O. Ignatyeva, C. S. Davies, D. A. Sylgacheva, A. Tsukamoto, H. Yoshikawa, P. O. Kapralov, A. Kirilyuk, V. I. Belotelov, and A. V. Kimel, Nat. Commun. **10**, 4786 (2019).

[19] S.-J. Im, C.-S. Ri, K.-S. Ho, and J. Herrmann, Phys. Rev. B **96**, 165437 (2017).

[20] K.-S. Ho, S.-J. Im, C.-S. Ri, J.-S. Pae, and G.-S. Song, Phys. Rev. B **101**, 041406(R) (2020).

[21] Q. Li, T. Wang, Y. K. Su, M. Yan, and M. Qiu, Opt. Express **18**, 8367 (2010).

[22] P. B. Johnson and R. W. Christy, Phys. Rev. B **6**, 4370 (1972).

[23] A. Dutta, A. V. Kildishev, V. M. Shalaev, A. Boltasseva, and E. E. Marinero, Opt. Mater. Express **7**, 4316 (2017).

[24] A. Davoyan and N. Engheta, Nat. Commun. **5**, 5250 (2014).

[25] See Supplemental Material at http://link.aps.org/supplemental/10.1103/PhysRevB.101.245420 for additional information about the transmission spectrum, the temporal coupled mode theory, cavity-size dependence of the resonant wavelength, and the power flow spectra for different distances between waveguide and cavity.

[26] C. Manolatou, M. J. Khan, S. Fan, P. R. Villenueve, H. A. Haus, and J. D. Joannopoulos, IEEE J. Quantum Electron. **35**, 1322 (1999).

[27] Q. Zhang, X.-G. Huang, X.-S. Lin, J. Tao, and X.-P. Jin, Opt. Express **17**, 7549 (2009).

[28] S.-J. Im, G.-S. Ho, D.-J. Yang, Z.-H. Hao, L. Zhou, N.-C. Kim, I.-G. Kim, and Q.-Q. Wang, Sci. Rep. **6**, 18660 (2016).

[29] S.-J. Im, J.-S. Pae, C.-S. Ri, K.-S. Ho, and J. Herrmann, Phys. Rev. B **99**, 041401(R) (2019).

[30] C.-S. Ri, S.-J. Im, J.-S. Pae, K.-S. Ho, Y.-H. Han, and J. Herrmann, Phys. Rev. B **100**, 155404 (2019).

[31] W. Cai, J. White, and M. L. Brongersma, Nano Lett. **9**, 4403 (2009).

[32] L. Chen, J. Shakya, and M. Lipson, Opt. Lett. **31**, 2133 (2006).

Correction: One of the original authors (Joachim Herrmann) requested that his name be removed, which has been implemented.